The Automatic Alignment System of the Virgo Interferometer

F. Acernese[6], P. Amico[10], M. Alshourbagy[11], F. Antonucci [12], S. Aoudia[7], P. Astone[12], S. Avino[6], D. Babusci[4], G. Ballardin[2], F. Barone[6], L. Barsotti[11], M. Barsuglia[8] , Th. S. Bauer[13], F. Beauville[1], S. Bigotta[11], S. Birindelli[11], M.A. Bizouard[8], C. Boccara[9], F. Bondu[7], L. Bosi[10], C. Bradaschia[11], S. Braccini[11], F. J. van den Brand[13],A. Brillet[7], V. Brisson[8], D. Buskulic[1], E. Calloni[6], E. Campagna[3], F. Carbognani[2], F. Cavalier[8], R. Cavalieri[2], G. Cella[11], E. Cesarini[3], E. Chassande-Mottin[7], N. Christensen[2], C. Corda[11], A. Corsi[12], F. Cottone[10], A.-C. Clapson[8], F. Cleva[7], J.-P. Coulon[7], E. Cuoco[2], A. Dari[10], V. Dattilo[2], M. Davier[8], M. del Prete[11], R. De Rosa[6], L. Di Fiore[6], A. Di Virgilio[11], B. Dujardin[7], A. Eleuteri[6], M. Evans[2], I. Ferrante[11], F. Fidecaro[11], I. Fiori[2], R. Flaminio[1,2], J.-D. Fournier[7], S. Frasca[12], F. Frasconi[11], L. Gammaitoni[10], F. Garufi[6], E. Genin[2], A. Gennai[11], A. Giazotto[11], G. Giordano[4], L. Giordano[6], R. Gouaty[1], D. Grosjean[1], G. Guidi[3], S. Hamdani[2], S. Hebri[2], H. Heitmann[7], P. Hello[8], D. Huet[2], S. Karkar[1], S. Kreckelbergh[8], P. La Penna[2], M. Laval[7], N. Leroy[8], N. Letendre[1], B. Lopez[2], Lorenzini[3], V. Loriette[9], G. Losurdo[3], J.-M. Mackowski[5], E. Majorana[12], C. N. Man[7], M. Mantovani[11], F. Marchesoni[10], F. Marion[1], J. Marque[2], F. Martelli[3], A. Masserot[1], M. Mazzoni[3], L. Milano[6], F. Menzinger[2], C. Moins[2], J. Moreau[9], N. Morgado[5], B. Mours[1], F. Nocera[2], C. Palomba[12], F. Paoletti[2], 11, S. Pardi[6], A. Pasqualetti[2], R. Passaquieti[11], D. Passuello[11], F. Piergiovanni[3], L. Pinard[5], R. Poggiani[11], M. Punturo[10], P. Puppo[12], S. van der Putten[13], K. Qipiani[6], P. Rapagnani[12], V. Reita[9], A. Remillieux[5], F. Ricci[12], I. Ricciardi[6], P. Ruggi [2], G. Russo[6], S. Solimeno[6], A. Spallicci[7], M. Tarallo[11], M. Tonelli[11], A. Toncelli[11], E. Tournefier[1], F. Travasso[10], C. Tremola[11], G. Vajente [11], D. Verkindt[1], F. Vetrano[3], A. Viceré[3], J.-Y. Vinet[7], H. Vocca[10] and M. Yvert[1]

[1]*Laboratoire d'Annecy-le-Vieux de Physique des Particules (LAPP), IN2P3/CNRS, Université de Savoie, Annecy-le-Vieux, France;*

[2]*European Gravitational Observatory (EGO), Cascina (Pi), Italia;*

[3]*INFN, Sezione di Firenze/Urbino, Sesto Fiorentino, and/or Università di Firenze, and/or Università di Urbino, Italia;*

[4]*INFN, Laboratori Nazionali di Frascati, Frascati (Rm), Italia;*

[5]*LMA, Villeurbanne, Lyon, France;*

[6]*INFN, sezione di Napoli and/or Università di Napoli "Federico II" Complesso Universitario di Monte S.Angelo, and/or Università di Salerno, Fisciano (Sa), Italia;*

[7]*Departement Artemis – Observatoire de la Côte d'Azur, BP 42209 06304 Nice, Cedex 4, France;*

[8]*LAL, Univ Paris-Sud, IN2P3/CNRS, Orsay, France*

[9]*ESPCI, Paris, France;*

[10]*INFN, Sezione di Perugia and/or Università di Perugia, Perugia, Italia;*

[11]*INFN, Sezione di Pisa and/or Università di Pisa, Pisa, Italia;*

[12]*INFN, Sezione di Roma and/or Università "La Sapienza", Roma, Italia.*

[13]*NIKHEF, NL-1009 DB Amsterdam and/or Vrije Universiteit, NL-1081 HV Amsterdam, The Netherlands*

The tuning and optimization of the angular control system represents one of the main activities of the Virgo commissioning. After a recall of the automatic alignment concepts and strategy, we describe the main results achieved, in terms of detector sensitivity and robustness. We will also describe the main limitations of the present scheme and the improvements planned in the near future.
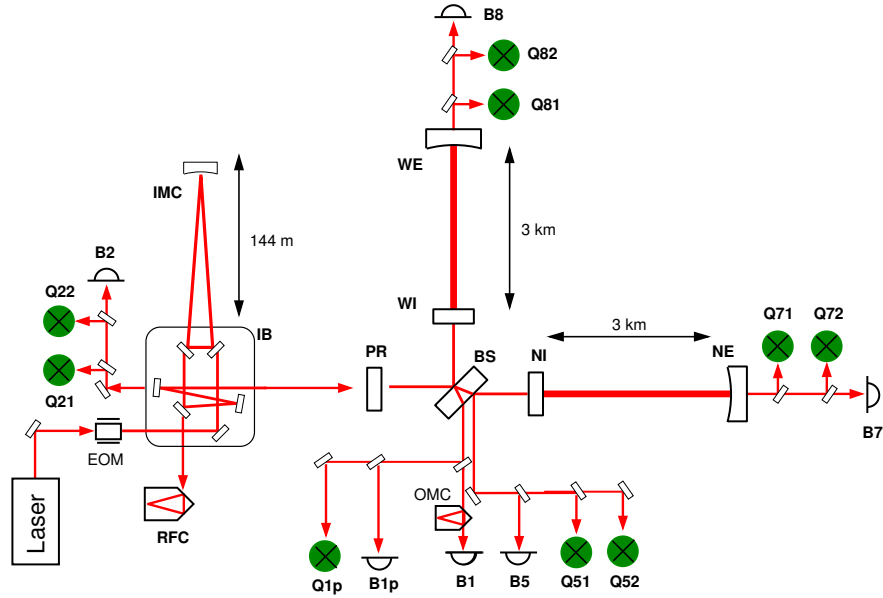
1 Optical Lay-Out and Loop Configuration

Figure 1: A simplified scheme of the optical design of Virgo in the final configuration. The photo-diodes used for longitudinal (labeled with **B**) and alignment (labeled with **Q**) control systems are shown. The gravitational wave signal is taken from B1.

The optical scheme of Virgo is shown in Fig. 1: the incoming laser beam is split by the *beam splitter* mirror (BS) in two beams which are injected into the two arm cavities (North arm and West arm). The longitudinal positions of all the mirrors are controlled such that there is destructive interference in the main output port (B1), called *dark fringe*. In this condition almost all the light power is reflected back to the *power recycling mirror* (PR).

A misalignment of the mirror with respect to the beam produces a variation on the effective arm length of the interferometer which can mimic the effect of a gravitational wave. Thus, to obtain the high sensitivity required for Virgo, the residual angular motion of the mirrors must be reduced down much below the micro-radiant level. The *automatic alignment* (AA) is a control system designed to maintain the overall global alignment of the optical elements, thus reducing the re-injected noise at the dark fringe port.

The Virgo AA system controls the angular pitch and yaw motion of the six main mirrors (PR, BS, NI, WI, NE, WE), and the input beam. The control scheme is based on the *wave front sensing technique* based on a modulation-demodulation scheme: the input beam is phase modulated and the diode signals are demodulated. We are using five beams coming out of the interferometer to construct angular error signals. They are: the main beam reflected by the ITF (Q2), the two beams transmitted at the end of the long arm cavities (Q7/8), the pick-off beam at the secondary surface of the BS (Q5) and the beam detected in the asymmetric port before the Output Mode Cleaner (Q1p),(see Fig. 1). In total we use 9 quadrant photo-diodes obtaining 27 error signals for each angular direction, two RF signals and one DC signal.

Initially all the mirrors are aligned with respect to local references by means of auxiliary devices, *Local control* (LC)[1], designed to drive the mirror alignment until the interferometer is dark-fringe locked. Then, if the fluctuations of the alignment are reduced to fractions of μrad
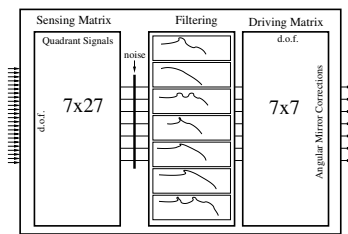
Figure 2: A schematic of the *Global Control System* with the sensing matrix (which converts the quadrant diode signals into mirror error signals), the filtering (which computes the correction to be sent to the mirrors) and the driving part which drives the mirror suspensions. Moreover between the Sensing Matrix and the Filtering we can inject colored noise.
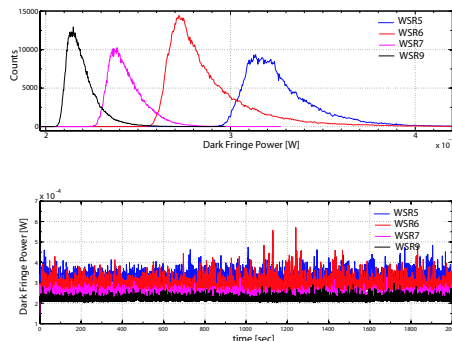

Figure 3: Dark Fringe power histogram (upper plot) and in time domain (lower plot) for the different *Weekly Science Runs*; we can notice a progressive improvement in stability and darkness of the dark port signal mainly due to the continuous improvement in the filtering path of the automatic alignment control chain.

direction	IB	PR	BS	NI	WI	Diff End	Comm End
θ_x	$Drift_{RF}$	$Fast_{RF}$	$Fast_{RF}$	$Drift_{DC}$	$Drift_{DC}$	$Fast_{RF}$	$Fast_{DC}$
θ_y	$Drift_{RF}$	$Fast_{RF}$	$Drift_{RF}$	$Drift_{DC}$	$Drift_{DC}$	$Fast_{RF}$	$Fast_{DC}$

Table 1: Configuration for the AA loops up to the WSR9. RF: demodulated error signal; DC: error signal given by the beam position on the quadrant diode.

the automatic alignment can be enabled.

The AA signals are processed by the *Global Control System* (Gc Fig. 2), which is a hardware and software system mainly constituted by: *Sensing Matrix*: 7×27 matrix for each direction, vertical or horizontal, which converts the quadrant signals into the angular motions; *Filtering*: which filters the AA error signals to construct the corrector signals; *Driving Matrix*: this is a 7×7 matrix, for each direction, vertical or horizontal, which sends the correction to the signals mirror suspensions, via coil/magnet actuators.

2   Commissioning

The full Automatic Alignment system has been implemented since the *C7* commissioning run, September 2005[2], we are controlling all the mirror angular degrees of freedom with two topologies of control: *Fast control*: bandwidth of a few Hz; *Drift control*: bandwidth of a few mHz with the *Local Control* still on: the auto-alignment error signal is added as an offset to the LC error point. We are using demodulated RF signals, which give the relative misalignment between the beam and the optical axes, and the DC signals which simply give the position of the beam on the quadrant diode. In Drift control mode the high frequency control is done by the local reference, in this way we are able to avoid the slow independent drift of the mirrors and maintain a good global alignment in the degrees of freedom which are less critical for noise propagation.

The commissioning of the AA system was focalized on several items as: the reduction of angular noise coupling into the dark fringe signal, the improvement of the robustness and stability of the system and the reproducibility of the alignment.

2.1   Optimization of the Control Filters

As we have shown before in the Fig. 2, in the *Global Control* the alignment correction filters are stored. In order to improve the loop performances it is important to optimize the filter shapes especially to:*high low frequency gain* in order to have a stable a robust global alignment
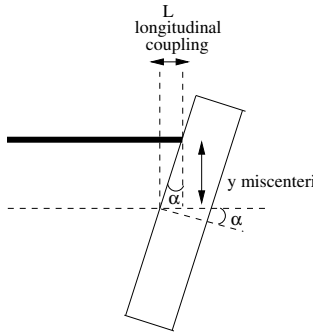
Figure 4: A schematic of the coupling mechanism between the angular misalignment and longitudinal signals if we have a miscentering of the beam on the mirror. y is the vertical miscentering, in this example, α is the mirror angular misalignment and L is the resulting longitudinal coupling.
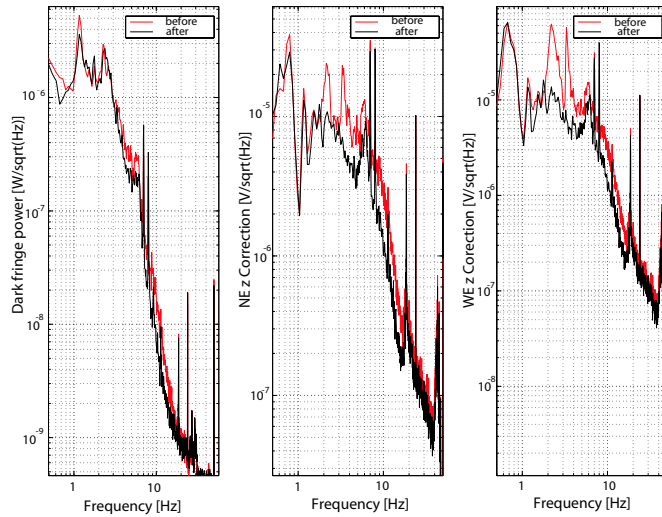

Figure 5: Comparison between the longitudinal correction signals for the North and West cavity (second and third plot respectively) before and after the beam centering (dotted and continuous curve respectively); we can notice how the corrections are reduced after the minimization, and this effects also the dark fringe power (first plot) reduction of noise coupling to the dark fringe is visible up to $\approx 20\,\text{Hz}$.

(suppress low frequency suspension motions); *strong high-frequency cut-off* in order to reduce the re-injection of alignment control noise into the dark fringe signal in the Virgo measurement bandwidth (10- 10 kHz).

Obviously the optimization of the control filter parameters is not trivial due to the fact that we have to be robust against variations in the interferometer, as for example during the *thermal transient* [4]. In this phase the interferometer signals which are used as error signals are very instable and therefore we need filters which have very large gain and phase margin.

For this reason we adopted the strategy to dynamically change the control filters during the lock acquisition, starting from simpler filters (with larger margins) trough more and more optimized filters.

The efforts on the filter optimization brought a clear improvement in the dark fringe stability as it is shown in Fig. 3, where we can see that the fringe is now darker and more stable.

2.2 Beam Centering on the Mirrors

One of the most direct mechanisms of coupling between the angular noise and the longitudinal signals can be generated by a miscentering of the beam on the mirror. As shown in Fig. 4, the longitudinal coupling is directly proportional to the miscentering of the beam on the mirror. For this reason a big effort of the commission activity has been put on the implementation on an automatic procedure of *beam centering*. After we have already engaged the alignment loops we inject a sinusoidal excitation to the end mirrors (with frequencies between 6 to 8 Hz). If the beam is not centered on the mirror, the sinusoidal excitation will be present also in the longitudinal error signal. We use this coupling as the error signal of our centering loop: we turn a little bit the input mirrors; with the AA system on, this shifts the beam position on the end mirrors. This is automated by a servo which minimizes the longitudinal coupling, in this way we have the beam centered with respect to the center of the longitudinal actuation point which is not necessary the center of the mirror, because it depends on the balancing of the actuator coils, but for the moment this was not a limiting factor.

The centering of the beam has a strong effect in the dark fringe signal as it is shown in

Fig. 5 in which we can clearly notice a noise coupling reduction up to some tens of Hz after the centering of the beams.

2.3   Second Modulation Frequency

Since the AA system was fully implemented, one of the main commissioning problems for this item was the lack of a RF signal for the control of the Common End mode, $((WE + NE)/2$, see Tab. 1). This degree of freedom was controlled by a DC signal, which depends on the relative position of the beam on the quadrant diode, which is then affected by bench drifts and local excitations. An RF signal, on the other hand, would give an absolute reference (relative misalignment between the beam and the ITF).

For solving this problem we designed a more complete control system (for which the simulations have shown a better controllability) adding an additional modulation frequency which does not enter into the interferometer, and control the common mode by using the quadrant diode in reflection from the recycling cavity (Q22 in Fig. 1).

We have implemented the additional modulation frequency since February 2007 and this allowed us to improve the overall global alignment and the repeatability of the lock.
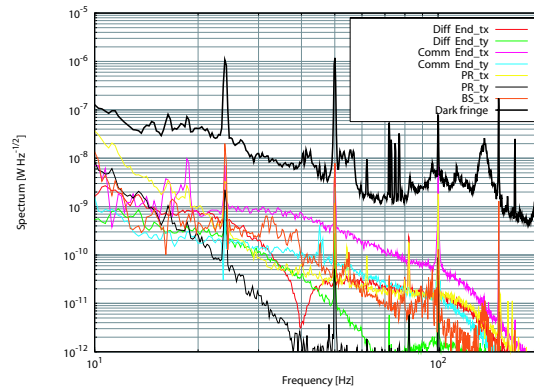
3   Conclusions

Figure 6: Alignment control noise projection measurement into dark fringe signal: we can see that alignment noise is presently not limiting the sensitivity curve.

Since the *C7* commissioning run in September 2005, when for the first time all the angular degrees of freedom were controlled, the commissioning of the Automatic Alignment system was dedicated to the improvement of the global alignment, the robustness and the reduction of the re-injection of control noise into dark fringe.

We have modified the original control design in order to avoid the lack of a demodulated signal for the Common end mirror alignment mode; moreover we have implemented a more flexible control system with correctors optimized for each phase of ITF switch-on, in order to survive during the initial *thermal transient*. We obtained a stable and robust system which is not presently limiting the sensitivity of the system.

References

1. F. Acernese *et al.* [Virgo Collaboration], "A local control system for the test masses of the Virgo gravitational wave detector", *Astrop. Phys.* **20** (2004) 617-628.
2. F. Acernese*et al.* [Virgo Collaboration], "The Virgo automatic alignment system", *C.Q.G.* **23** (2006) S91-S102.
3. D. Babusci, H. Fang, G. Giordano, G. Matone, L. Matone, V. Sannibale, "Alignment procedure for the VIRGO interferometer: experimental results from the Frascati prototype", *Phys. Lett. A* **226**, 31–40 (1997).
4. F. Acernese*et al.* [Virgo Collaboration], "Status of Virgo", in this proceeding series.